Low-temperature heat-capacity study of the U_6X ($X \equiv$ Mn, Fe, Co, Ni) compounds

K. N. Yang and M. B. Maple
Department of Physics and Institute for Pure and Applied Physical Sciences, University of California, San Diego, La Jolla, California 92093

L. E. DeLong and J. G. Huber*
Department of Physics and Astronomy, University of Kentucky, Lexington, Kentucky 40506-0055

A. Junod
Département de Physique de la Matière Condensée, Université de Genève, CH-1211 Genève 4, Switzerland
(Received 26 May 1988)

Measurements of the superconducting- and normal-state heat capacity of U_6X ($X \equiv$ Mn, Fe, Co, Ni) compounds have been performed over a temperature range 1 K $\lesssim T \lesssim$ 35 K. The U_6X compounds have strong renormalizations of the free-carrier effective mass m^* in the range $10m_e \lesssim m^* \lesssim 50m_e$ ($m_e \equiv$ free-electron mass). The unusual magnitude and temperature dependence of the U_6X heat capacities suggest the presence of high densities of low-energy excitations of undetermined nature. The results are analyzed in terms of models appropriate to heavy-fermion liquids, and anisotropic or strong-coupled superconductors. The U_6X compounds form a link between relatively low-m^*, high-transition-temperature $A15$ compounds and the more extreme examples of heavy-fermion superconductors such as UBe_{13}, UPt_3, and $CeCuSi_2$ for which $m^* \sim 10^2 m_e$.

I. INTRODUCTION

The U_6X ($X \equiv$ Mn, Fe, Co, Ni) phases are among the earliest known U superconductors and include the first examples of superconducting Fe or Mn compounds.[1] In spite of their content of ferromagnetic $3d$ elements and strong paramagnetism,[2–5] the highest-known upper critical magnetic field H_{c2} and superconducting transition temperature T_c for U compounds are observed within this class of materials.[6] Indeed, these compounds have long been cited as intriguing examples of the puzzling interplay between magnetism and superconductivity.[7–10] Recently, U_6Fe was observed[11–13] to exhibit anomalous low-temperature properties that were attributed to "heavy fermions"[14] resulting from the hybridization between localized $5f$ and itinerant conduction electron states.[15]

Measurement of the low-temperature heat capacity has proven to be a very useful method of characterizing the strength and character of the many-body correlations between heavy-fermion quasiparticles.[16] The magnitude and temperature dependence of the low-temperature electronic contribution of the normal-state heat capacity reflect the magnitude of the fermion effective mass m^* and low-energy structure in the quasiparticle density of states. Measurements at and below T_c are crucial in proving the bulk nature of the superconducting state and provide useful constraints on parameters characterizing the heavy quasiparticles.[12–14]

We have performed measurements of the low-temperature heat capacity of the U_6X ($X \equiv$ Mn, Fe, Co, Ni) compounds. Analyses of the resulting data indicate that these materials have strong renormalizations of the fermion mass in the range $10 \lesssim m^*/m_e \lesssim 50$ ($m_e \equiv$ free-electron mass). The temperature dependences of the U_6X heat capacities generally reflect the presence of a high density of low-energy excitations of undetermined nature. The data are consistent with a picture in which the U_6X compounds are exchange-enhanced paramagnets that form a link between narrow-band transition metals—particularly high-T_c $A15$ compounds—and heavy-fermion superconductors such as UBe_{13} (Ref. 17) and UPt_3.[18]

II. EXPERIMENTAL DETAILS

Samples were prepared from high-purity starting materials by arc melting in a pure argon atmosphere. A Zr getter was melted several times, followed by several cycles of melting, turning, and remelting of the U-X charge on a water-cooled copper hearth. A slight excess of U was used in the sample melt in order to suppress the amount of UX_2 phase that is introduced in the peritectic formation of all of the U_6X compounds.[19] After removal from the arc furnace, the samples were wrapped in Ta foil and sealed in evacuated quartz ampoules and annealed at temperatures just below the peritectics. Details of the sample preparation are summarized in Table I.

Routine x-ray diffraction scans of the U_6Mn, U_6Co, and U_6Ni materials studied herein were conducted on unannealed powder samples. The diffraction peaks were broad and poorly resolved, but could be completely indexed in terms of the majority U_6Mn-type structure,[19] although a few weak peaks were explained as due to U oxides or $C15$-type, UMn_2 (in the case of the U_6Mn sample, only) phase.[19] The short penetration depth of x rays in U

TABLE I. Selected experimental properties of U_6X samples used in the present study.

Compound stoichiometry	Sample designation	Starting materials	V_m[a] (cm^3)	T_c[b] (K)	ΔT_c[c] (K)	Anneal
$U_{6.15}Mn$	II-46	U: Atomergic, 3-9's, No. U022Cl752 Mn: Johnson-Matthey, "puratronic" grade	84.167	2.19	0.55	11 d 500–700 °C
$U_{6.10}Fe$	II-33[d]	U: Alfa Products, 3-9's, No. 100677 Fe: Alfa Products, 3-9's No. 062278	83.703	3.764	0.136	10 d, 660–770 °C
$U_{6.05}Co$	II-39*B*	U: Alfa Products, 3-9's, No. 100677 Co: Jarrell-Ash, "high purity"	83.319	2.08	1.47	14 d, 600–760 °C
$U_{6.05}Ni$	II-49*B*	U: Alfa Products, 3-9's, No. 100677 Ni: Alfa Products 3-9's	83.838	0.50	0.22	7 d, 500–730 °C

[a]After Ref. 20.
[b]Inductively determined. Unannealed powder was prepared from C_P samples for U_6Mn, U_6Co, U_6Ni; U_6Fe data was obtained from a piece cut from the C_P sample.
[c]Difference in the temperatures at which the inductive transition signal reached 10% and 90% completion.
[d]Same sample studied in C_P and H_{c2} measurements reported in Refs. 11–13.

compounds and the strain broadening expected in powder samples of the U_6X phases[5] can account for the poor quality of the x-ray data. Broadening of the inductively measured superconducting transitions of unannealed powder samples of U_6Mn, U_6Co, and U_6Ni (see Table I) has also been observed.

Our U_6Fe sample No. II-33 is the same one studied in the heat capacity, H_{c2}, and electrical resistivity measurements reported in Refs. 11–13. X-ray diffraction and metallography studies were conducted on this sample with contributions by Roof and Pereyra of Los Alamos National Laboratory. Sample II-33 was found to be at least 95% single phase from x-ray measurements, although more sensitive metallography work detected small amounts of U oxide inclusions and excess U lodged at grain boundaries.[12,13] Engelhardt[20] and White *et al.*[21] have done extensive work on the effects of stoichiometry and annealing on the T_c's of U_6X compounds. A detailed discussion of impurity phases present in U_6X compounds is included in a report[5] of magnetization measurements on sample II-33 and other U_6X materials, and will not be discussed further here.

Heat-capacity measurements were performed using a semiadiabatic heat-pulse calorimeter with a mechanical heat switch. The calorimeter was attached to a ^{3}He evaporation refrigerator providing an experimental temperature range 0.85 K $\lesssim T \lesssim$ 35 K in applied magnetic fields of zero and 2 kOe. Details of the methods used in analyzing the calorimetric data are given in Sec. III.

Magnetization measurements were performed on a section of the U_6Mn sample II-46, only. An SHE (Biotechnologies, Inc.) magnetometer was used to cover the temperature range 2 K $\lesssim T \lesssim$ 300 K and applied magnetic fields $0 \leq H \leq 2.0$ T. Demagnetization and anisotropy effects were neglected in these measurements and the associated analysis.

III. METHODS OF DATA ANALYSIS

The "strong form" of the third law of thermodynamics implies that the entropy S can be related to the constant-volume heat capacity C_V via

$$S(T) = \int_0^T \frac{C_V}{t} dt \ , \tag{1}$$

where $S(0) \equiv 0$. Most experimental heat-capacity measurements, on the other hand, yield data for the constant-pressure heat capacity C_P. These results can, in principle, be used to calculate the more fundamental quantity C_V through the relation

$$C_P - C_V = VT\frac{\alpha_P^2}{\kappa_T} \ , \tag{2}$$

where α_P is the isobaric thermal expansion coefficient and κ_T is the isothermal compressibility. However, the difference between C_P and C_V is usually less than 1% for most metals below room temperature,[22] and is generally neglected in the analysis of experimental results. We will therefore assume in this paper that our C_P data accurately reflect the behavior of C_V.

There are several methods of analysis which can be employed to extract important physical parameters from experimental heat capacity data for metals. We have chosen to apply two quite different methods that are reasonably representative of the more familiar models of the thermal behavior of superconductors. We will describe the strengths and weaknesses of each of these methods, and summarize and compare the numerical results that they yield.

A. Polynomial method

The results of low-temperature normal-state heat-capacity measurements are frequently analyzed by fitting

data to a low-power polynomial of the form

$$C_{Vn}=\gamma^*T+\beta T^3+\alpha T^5 \ . \tag{3}$$

γ^* is the electronic coefficient given by

$$\gamma^*=\frac{2\pi^2}{3}k_B^2N^*(E_F) \ , \tag{4}$$

where $N^*(E_F)$ is the renormalized electronic density of states at the Fermi energy, and the coefficient β of the low-temperature phonon term is given by

$$\beta=\frac{12\pi^4N_Ak_Bn}{5\theta_D^3} \ , \tag{5}$$

where N_A is Avogadro's number, θ_D is the Debye temperature and $n=$ number of atoms per formula unit. The α coefficient is best considered as a fitting parameter that approximates finite-temperature corrections to the low-temperature behavior of the electron and lattice systems. Some care must be exercised in applying the model of Eqs. (3)–(5) to particular metals. Strictly speaking, Eq. (3) should not be applied at temperatures $T\gg\theta_D/50$ (Ref. 23), or in situations where γ^* is effectively "temperature dependent" as is the case in UPt_3, UBe_{13}, $CeCu_2Si_2$, and certain other heavy-fermion materials.[16]

Analyses performed on superconducting-state data must deal with the finite discontinuity ΔC in heat capacity at T_c. This discontinuity is always broadened in laboratory situations due to the presence of coexisting normal and superconducting regions in imperfect sample materials within a temperature interval ΔT_c about the ideal transition point. Therefore, we have chosen to initially integrate the experimental data according to Eq. (1) in order to obtain the superconducting-state entropy $S_s(T)$. This procedure has several advantages. First, since the normal-state entropy S_n satisfies the relation $S_n(T_c)=S_s(T_c)$, the errors introduced by fitting the *integrated* C_V data near T_c are minimal. Second, the entropy relation at T_c provides a useful constraint on the parameters derived from the fits of $S_n(T)$ conducted over finite-temperature intervals. Third, the entropy difference $\Delta S=S_n-S_s$ is also required in calculating the behavior of the thermodynamic critical field H_c. Of course, a realistic extrapolation of $S_s(T)$ as $T\rightarrow0$ is required, similar to the normal-state case.

The superconducting-state heat capacity is assumed to have the form [see the discussion of Eqs. (27) and (28)]

$$C_{Vs}=Ae^{-B/T}+\beta T^3+\alpha T^5 \ . \tag{6}$$

We note that this form is not strictly valid (especially for strong-coupled materials), but should provide a reasonably accurate extrapolation of C_{Vs} in the absence of anomalous low-temperature behavior [such as observed for $(U_{1-x}Th_x)Be_{13}$ alloys (Ref. 24)].

An iterative method was employed to obtain self-consistent fits for both the normal- and superconducting-state data. The procedure can be broken down into several steps.

(1) "Zeroth-order" approximations $\alpha=\alpha_0$ and $\beta=\beta_0$ are obtained from fits of the data to Eq. (3) over limited temperature intervals extending above T_c where $C_{Vn}T^{-1}$ versus T^2 plots are nearly linear.

(2) The β_0 and α_0 parameters of step (1) are used to calculate the electronic contributions C_{es} to C_{Vs} where

$$C_{es}\equiv A_0e^{-B_0/T}=C_{Vs}-\alpha_0T^5-\beta_0T^3 \ . \tag{7}$$

A linear, least-squares fit of the processed data of $\ln C_{es}$ versus T^{-1} yields the parameters A_0 and B_0 for "zeroth order."

(3) The parameters α_c, β_0, A_0, and B_0 are then used to calculate the entropy for $T=T_{\min}$, the lowest measuring temperature:

$$S_{\min}=A_0\int_0^{T_{\min}}\frac{e^{-B_0/t}}{t}dt+\tfrac{1}{3}\beta_0T_{\min}^3+\tfrac{1}{5}\alpha_0T_{\min}^5 \ . \tag{8}$$

(4) The entropy of the sample is then calculated for $T>T_{\min}$ using experimental data and $S_{\min}$:

$$S(T)=S_{\min}+\sum_{i=0}^{N-1}\frac{1}{2}\left[\frac{C_i}{T_i}+\frac{C_{i+1}}{T_{i+1}}\right](T_{i+1}-T_i) \ . \tag{9}$$

(5) The $S(T)$ obtained from step (4) is then used to recalculate the parameters α and β using

$$C_{Vn}(T)-S_n(T)=\tfrac{2}{3}\beta T^3+\tfrac{4}{5}\alpha T^5 \tag{10}$$

at each temperature experimentally investigated. A linear, least-squares fit of $(C_{Vn}-S_n)T^{-3}$ versus T^2 yields new values of α and β as input for step (2) above.

(6) The steps (2)–(5) are repeated, yielding new values of A, B, and $S_{\min}$, until all parameters converge to within 0.1%.

(7) The value of γ^* is determined from the final results of step (6) using

$$\gamma^*T=S_n(T)-\tfrac{1}{3}\beta T^3-\tfrac{1}{5}\alpha T^5 \ . \tag{11}$$

The thermodynamic critical field can be calculated from

$$\frac{1}{8\pi}[H_C^2(T)-H_c^2(0)]=-V_m^{-1}\int_0^T\Delta S(t)dt \ , \tag{12}$$

where V_m is the molar volume,

$$\frac{H_c^2(0)}{8\pi}=V_m^{-1}\int_0^{T_c}\Delta S(t)dt \ , \tag{13}$$

$$\Delta S(T)=\gamma^*T+\tfrac{1}{3}\beta T^3+\tfrac{1}{5}\alpha T^5-S(T) \ , \tag{14}$$

and $S(T)$ is taken from the final iteration's results in Eq. (9).

Several elementary models of superconductivity predict the following approximate form for $H_c(T)$ at $T\ll T_c$ (Ref. 25):

$$H_c(T)=H_c(0)[1-(T/T_c)^2] \ . \tag{15}$$

The results of Eq. (12) were fitted to Eq. (15) using the method of least squares. The best-fit value of $H_c(0)$ was then compared to that obtained from the experimental data using the low-temperature extrapolation of Eq. (7) with Eq. (13).

B. Phonon moment method

Analytical techniques for extracting important information from the lattice specific-heat data for metals have appeared in recent years.[26,27] These are particularly useful in the case of superconductors since the traditional electron-phonon interaction mechanism for superconductivity implies that important physical parameters such as T_c, Δ, and λ will depend upon the phonon and electronic densities of states. These techniques can be invaluable in situations where inelastic electron tunneling or neutron scattering measurements are difficult or impossible to make. Further, recent model calculations for strong-coupled superconductors have demonstrated that T_c's can be quantitatively estimated from a knowledge of various frequency moments $\langle\omega^n\rangle$ of the phonon spectrum.[26-28]

The $\langle\omega^n\rangle$ are defined in terms of the phonon density of states $F(\omega)$ by

$$\langle\omega^n\rangle=\int\omega^n F(\omega)d\omega\ , \tag{16}$$

which is an expression that is difficult to compare with experiment. However, it can be shown that the $\langle\omega^n\rangle$ can be directly obtained from lattice heat-capacity data without resort to detailed measurements of phonon dispersion curves.[29] Some of the superconducting properties can then be calculated with the aid of the Allen-Dynes formula:[28]

$$T_c=\frac{f_1 f_2}{1.20}\omega_{\log}\exp\left[\frac{1.04(1+\lambda)}{\mu^*+0.62\lambda\mu^*-\lambda}\right]\ . \tag{17}$$

Here, the parameter $\omega_{\log}$ is a characteristic phonon scaling frequency given by

$$\omega_{\log}=\exp\left[\frac{2}{\lambda}\int\alpha^2F(\omega)\ln\omega\, d\ln\omega\right]\ , \tag{18}$$

and the electron-phonon coupling λ is calculated from

$$\lambda=2\int\alpha^2F(\omega)\,d\ln\omega\ . \tag{19}$$

$\omega_{\log}$ cannot be directly calculated from heat-capacity data without making additional assumptions concerning the frequency dependence of the electron-phonon spectral function $\alpha^2F(\omega)$. Fortunately, previous experiments and analyses[28] have shown that $\omega_{\log}\approx\bar{\omega}_{\log}$, where

$$\bar{\omega}_{\log}\equiv\exp\left[\frac{\int F(\omega)\ln\omega\, d\ln\omega}{\int F(\omega)\,d\ln\omega}\right]\ . \tag{20}$$

A schematic form for $F(\omega)$ can be obtained by fitting the frequency moments obtained from heat-capacity data to the following expression:

$$\langle\omega^n\rangle=\frac{\int F(\omega)\omega^n\,d\omega}{\int F(\omega)\,d\omega}\ . \tag{21}$$

Note that a customary normalization sets $\int F(\omega)d\omega=1$. Using the facts that the functions f_1 and f_2 are near unity for $\lambda\lesssim1.5$, and the Coulomb pseudopotential $\mu^*\approx0.1$ for transition metals, one obtains a reasonably quantitative relation between T_c, λ, and the heat-capacity data:

$$T_c\frac{\bar{\omega}_{\log}}{1.2}\exp\left[\frac{1.04(1+\lambda)}{\mu^*+0.62\lambda\mu^*-\lambda}\right]\ . \tag{22}$$

Although there are no particular assumptions which must be made concerning the detailed behavior of $F(\omega)$, in practice it is sufficient to assume a four- to six-parameter model spectrum of the form

$$F(\omega)=\sum_i D_i F_D(\omega/\theta_i)\ , \tag{23}$$

where F_D is an elementary Debye spectrum characterized by a "partial Debye temperature" θ_i (Ref. 27):

$$F_D(\omega/\theta_i)=\begin{cases}3\omega^2\theta_i^{-3}, & \omega\le\theta_i\\ 0, & \omega>\theta_i\ .\end{cases} \tag{24}$$

The fitting procedure is constrained by the normalization condition $\sum D_i=1$ (equivalent to the fact that the high-temperature lattice heat capacity $\rightarrow3R$), and the entropy constraint on the electronic heat capacity at T_c. This procedure has been found to yield values of $\langle\omega^n\rangle$ and $\bar{\omega}_{\log}$ that compare favorably with the results of tunneling and neutron scattering experiments for $A15$ compounds.[30,31] The procedure is initially aided by the fact that $[C(T)-\gamma^*T]T^{-3}$ is an approximate image of the spectral weight $D(\omega)-\omega^{-2}F(\omega)$ for $\hbar\omega\approx5k_BT$ (Refs. 27, 29, and 30). The rms deviations of the data from the best-fit model heat capacities derived from Eq. (23) are $\sim1\%$.

The phonon moment method we have used is subject to a number of important assumptions. All of the contributions to $C_{Pn}(T)$ except the electronic term γ^*T are assumed to be phononic in origin; otherwise, our procedure may be viewed as a convenient way to analyze the normal-state data over a wide temperature range [where Eq. (3) fails] using only a small number of adjustable parameters. The assumption of a composite Debye spectrum for $F(\omega)$ ignores anharmonicity. However, considerably more detail and additional assumptions must be incorporated into this type of analysis in order to approximate anharmonic effects,[26,32] and we have neglected them in the fitting procedure.

TABLE II. Parameters derived from a polynomial analyses of the normal- and superconducting-state heat capacities of U_6X compounds.

Compound	Temperature interval of fit	γ^* (mJ/mol K^2)	β (mJ/mol K^4)	θ_D (K)	α (mJ/mol K^6)	A (mJ/mol K)	B (K)
U_6Mn	3 K $\le T\le$ 5.75 K	98.81	1.819	195.6	8.911×10^{-2}	2252	3.452
U_6Fe	4.2 K $\le T\le$ 10.2 K	151.7	9.104	114.3	-3.045×10^{-2}	4396	5.947
U_6Co	2.6 K $\le T\le$ 5.5 K	129.7	9.809	111.5	-8.672×10^{-2}	3310	3.732
U_6Ni	0.85 K $\le T\le$ 5.0 K	91.36	2.375	178.9	$\gtrsim0$		

IV. EXPERIMENTAL RESULTS AND ANALYSIS

The experimental data for $C_P T^{-1}$ are plotted versus T^2 for each of the U_6X compounds in Figs. 1 and 2. There is marked nonlinear character in these plots at $T \geq 5$ K, as shown in Fig. 3. This behavior implies that a high density of low-energy excitations (e.g., "soft" phonons or paramagnons) dominates the heat capacity of these materials. The strong negative curvature at modest temperatures in $C_P T^{-1}$ versus T^2 is very similar to the data for high-T_c, high-H_{c2}, $A15$, and Chevrel phase materials.[26,30,33] However, the overall magnitudes of the heat capacities of the U_6X compounds are several times larger than many high-T_c materials, and are more than an order of magnitude larger than those of simple metals such as Cu.[5,22,23]

A. Polynomial analysis

Extreme care must be exercised in the use of the polynomial ("POLY") method to extract physical parameters relevant to the U_6X materials. Specifically, the POLY analysis must be restricted to a narrow temperature interval above T_c where the curvature of $C_{Pn} T^{-1}$ versus T^2 is relatively insignificant. The best-fit parameters from the POLY analysis of the normal- and superconducting-state data are summarized in Table II.

Comparisons of the experimental data and the best-fit predictions of Eqs. (3) and (6) are given in Fig. 3. We note that the transition anomaly at T_c is relatively broad in the case of U_6Mn. This is probably due to the poorer quality of U used in preparing this sample and the relatively high vapor pressure of Mn in the melt. Peculiarities in the metallurgy and lattice parameters of U_6Mn have been noted earlier.[8,20] Unfortunately, a significant transition width introduces uncertainties in the estimation of the jump $\Delta C_P(T_c)$ in heat capacity at T_c and the intrinsic behavior of $H_c(T)$, not to mention T_c itself.

We have defined a calorimetric width δT_c of the transition by noting the temperatures of the peak in C_{Ps} and the intersection of the extrapolations of C_{Pn} (given by the parameters of Table II) and the quasilinear-T region of the transition anomaly. A minimum value $\Delta C_P^{\min}$ of $\Delta C_P(T_c)$ can be estimated from the difference in C_{Ps} at the peak of the anomaly and C_{Pn} near the onset of the transition anomaly. This number can be compared to an "ideal" value, $\Delta C_P^{\text{ideal}}$ determined by extrapolating $C_{Ps}(T < T_c)$ and $C_{Pn}(T > T_c)$ into the transition region. An estimate $T_c(\text{cal})$ for T_c is obtained from a graphical analysis of a $C_P T^{-1}$ versus T plot. $T_c(\text{cal})$ is adjusted until the entropy difference $\Delta S(T)$ [see Eq. (14)] estimated from the actual data near $T_c(\text{cal})$ and an idealized, sharp transition anomaly at $T_c(\text{cal})$, are equal.

Additional estimates of T_c can be extracted from fits of $H_c(T)$ to the "parabolic law" of Eq. (15) (yielding "T_c^{pb}"), and by extrapolating the calculated values of $H_c(T)$ and

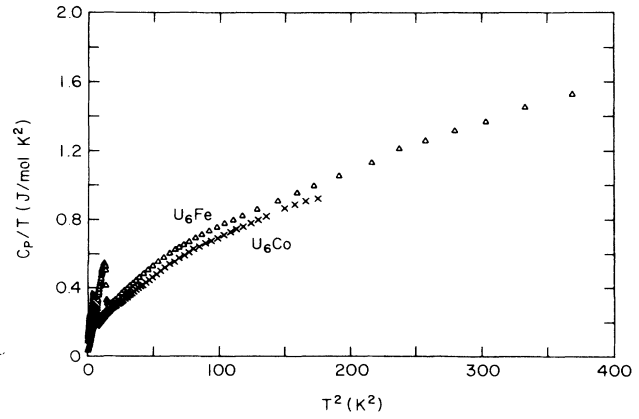

FIG. 1. Heat capacity C_P divided by temperature T vs T^2 for U_6Fe and U_6Co.

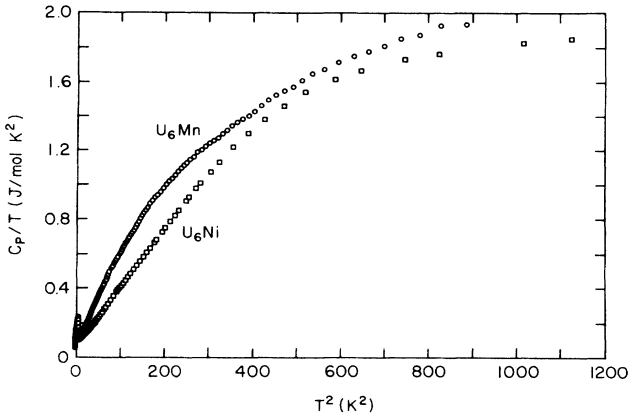

FIG. 2. Heat capacity C_P divided by temperature T vs T^2 for U_6Mn and U_6Ni.

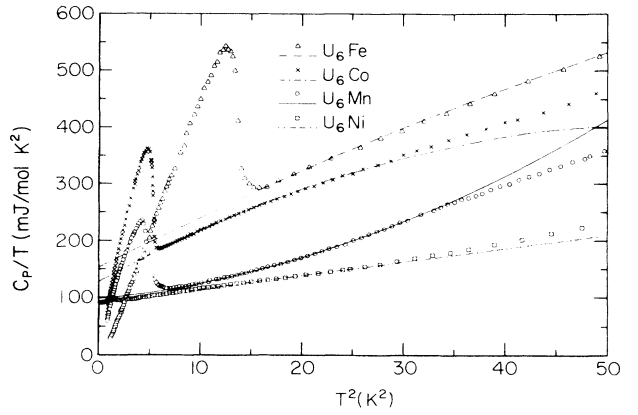

FIG. 3. Heat capacity C_P divided by temperature T vs T^2 for U_6X (X=Mn, Fe, Co, Ni) compounds. Experimental data are represented by the points, and fits of the data by the polynomial method are represented by the lines. Details of the fit parameters are given in Table II. The polynomial method provides an excellent fit for the normal-state U_6Fe data for $T \lesssim 10$ K, whereas the method is successful only for $T \lesssim 5.5$ K in the case of the other compounds.

TABLE III. Additional superconducting-state parameters derived from polynomial analyses of the heat capacities of U_6X compounds.

Compound	T_c (cal) (K)	δT_c (K)	$\Delta C_P^{\min}$ (mJ/mol K)	$\Delta C_P^{\text{ideal}}$ (mJ/mol K)	S_s ($T_{\min}$) (mJ/mol K)	$T_{\min}$ (K)	$\frac{\Delta C_P(T_c)^a}{\gamma^* T_c}$
U_6Mn	2.21 ±0.01	0.275	223.7	344.8	22.255	0.925	1.6
U_6Fe	3.695±0.01	0.250	854.5	1197	7.407	1.110	2.1
U_6Co	2.29 ±0.01	0.165	368.9	513.0	14.54	0.925	1.7

[a]Calculated using $\Delta C_P^{\text{ideal}}$ and T_c(cal), and γ^* (from Table II).

$\Delta S(T)$ [from Eqs. (12) and (14)] to H_c or $\Delta S=0$ at "T_c^{th}." Additional parameters, chiefly relevant to the superconducting state, are collected in Table III. The data for $\Delta C_P(T_c)/\gamma^* T_c$ show evidence for strong coupling (compared to a BCS value of 1.43), particularly in the case of U_6Fe.

Measurements of the thermodynamic critical field $H_c(T)$ can also provide additional information concerning the coupling strength and the quality of the fits. Plots of $H_c(T)$ versus T, as calculated from Eq. (12), are shown in Fig. 4. Various parameters concerning $H_c(T)$ are summarized in Table IV. The tabulated values of the ratio $H_c^2(0)/\gamma^* T_c^2$ are to be compared to the BCS ratio, 5.94. These ratios corroborate the evidence for strong-coupling renormalizations of $\Delta C_P(T_c)/\gamma^* T_c$ values listed in Table III: U_6Mn appears to be BCS-like, while U_6Co is moderately strong coupled and U_6Fe is substantially strong coupled. The close agreement between various estimates of T_c and $H_c(0)$ for each compound indicates that the fitting procedure is satisfactory. However, we note that the relatively poor quality of the U_6Mn sample is clearly reflected in the strong positive curvature of $H_c(T)$ near a poorly-defined T_c.

Another check of the fitting procedure can be made by comparing the low-temperature behavior of the superconducting-state data C_{Ps} to the extrapolation formula of Eq. (6). We define the electronic contribution to the superconducting-state heat capacity by

$$C_{es} \equiv C_{Ps} - \beta T^3 - \alpha T^5 \ . \tag{25}$$

Plots of $\ln[C_{es}/\gamma^* T_c]$ versus T_c/T for U_6Mn, U_6Fe, and U_6Co are shown in Fig. 5. These data can be compared to BCS model predictions where

$$\frac{C_{es}}{\gamma^* T_c} \approx 8.5 \exp(-1.44 T_c/T) \tag{26}$$

for $2.5 \lesssim T_c/T \lesssim 6$ (Ref. 25). Comparisons of the data of

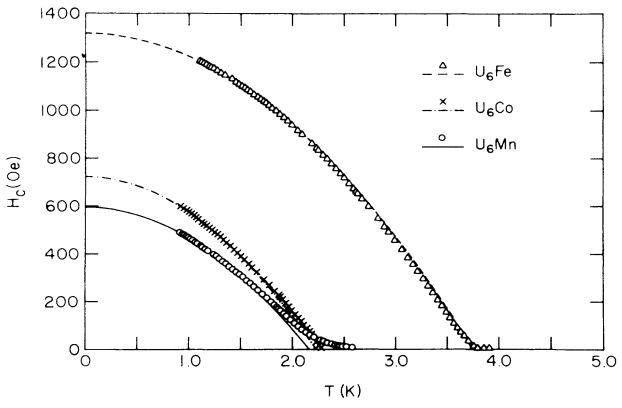

FIG. 4. Thermodynamic critical field H_c vs temperature T for U_6Mn, U_6Fe and U_6Co. Points were calculated from the experimental data using Eq. (12), as described in the text. The lines represent fits of the $H_c(T)$ points to the parabolic form of Eq. (15). Relevant parameters are collected in Table IV.

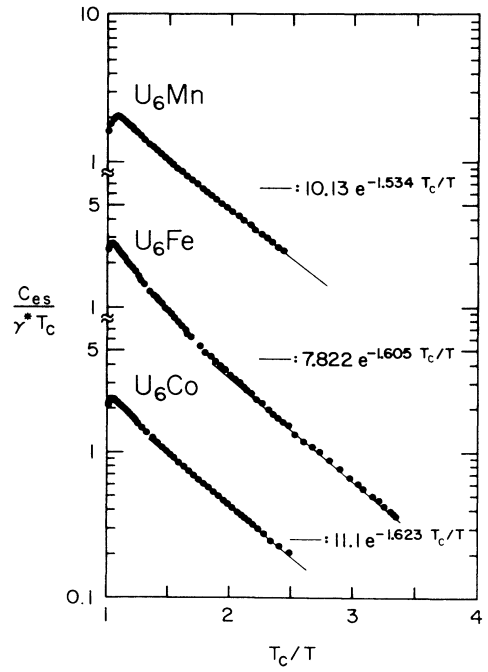

FIG. 5. Electronic contribution C_{es} to the superconducting-state heat capacity divided by the normal-state electronic heat capacity $\gamma^* T_c$ at the transition temperature T_c vs T_c divided by temperature T for U_6Mn, U_6Fe, and U_6Co. The points were derived from experimental data using Eq. (25), as described in the text. The solid lines represent fits of the points to Eq. (26) over the temperature range 0.9–1.5 K.

TABLE IV. Thermodynamic critical field parameters derived from polynomial analyses of the heat capacities of U_6X compounds.

Compound	T_c^{th} [a] (K)	$H_c(0)$ [b] (Oe)	T_c^{pb} [c] (K)	$H_c(0)$ [c] (Oe)	$\frac{V_m H_c^2(0)}{\gamma^* T_c^2}$ [d]
U_6Mn	2.25 ±0.05	598.1	2.156	595.8	5.97
U_6Fe	3.705±0.015	1312	3.746	1317	6.97
U_6Co	2.30 ±0.01	721.2	2.225	723.3	6.37

[a]Estimated from linear extrapolations of $H_c(T)$ and $\Delta S(T)$ data and T_c(cal) from Table III.
[b]Calculated from Eq. (12).
[c]Derived from fits of the $H_c(T)$ data to Eq. (15), as described in the text.
[d]Calculated in Gaussian units using T_c^{th}, and $H_c(0)$ from Eq. (12).

Fig. 5 to fits using Eq. (26) are also shown in Fig. 5.

The precise form of the temperature dependence of the superconducting energy gap $\Delta(T)$ may cause deviations from Eq. (26) near T_c, and gap anisotropy or strong-coupling effects may cause additional deviations at very low temperatures.[25,34,35] The data for U_6Mn and U_6Co are well fitted by Eq. (26) to rather high temperatures [outside the expected range of validity of Eq. (26)], and U_6Fe exhibits a BCS-like behavior over the expected temperature range. The quality and self-consistency of the fits using Eq. (6) are strongly supported by the results shown in Fig. 5. Lower-temperature measurements of C_{Ps} for U_6X compounds would be desirable in view of recent claims[36,37] that the non-BCS behavior of C_{es} in UBe_{13} provides clear evidence for triplet pairing.

B. Phonon moment analysis

Results of the fits of the heat-capacity data of U_6X compounds over a wide temperature range using the phonon moment ("MOM") analysis are summarized in Table V. Plots of $C_P T^{-1}$ versus T are shown in Fig. 6, along with the behavior calculated for selected "best" fits. The parameters relevant to the model curves shown in Fig. 6 are collected in Table VI. The agreement between the values of γ^* and Θ_D from the POLY analysis (see Table II) and the average values of γ^* and $\Theta(T\rightarrow 0)$ from the MOM analysis (see Table V) is excellent.

Our analyses indicate that the small, systematic differences between the corresponding parameters given in Tables II and V are primarily due to differing estimates of $S_{\min}$ [see Eq. (8)] obtained in the two methods used to fit the data. $S_{\min}$ is estimated in the MOM method by fitting the first 5–10 superconducting-state data at $T > T_{\min}$ to a form $C_s = \zeta T^3 + \eta T^5$, yielding $S_{\min} = \frac{1}{3}\zeta T_{\min}^3 + \eta T_{\min}^5$. This procedure will generally overestimate $S_{\min}$, leading to systematically higher γ^* values compared to the POLY method. Note also that the POLY method gives a much stronger weight to lower-temperature data due to the reduced size of the fitting interval and strict enforcement of the entropy constraint at T_c. The MOM method treats all of the data with equal weight. Additional calculations of T_c and $H_c(T)$ within the MOM analysis are in excellent agreement with the POLY results quoted earlier and will not be detailed here.

The *qualitative* nature (e.g., the relative weight of low-frequency modes) of the $D(\omega)\sim\omega^{-2}F(\omega)$ required to fit the heat-capacity data for the U_6X samples can be inferred from our analyses; whereas it is important to note that several *quantitatively* different model $F(\omega)$'s have been shown previously to provide equally satisfactory fits of the data for $A15$ materials.[30] Plots of $\omega^{-2}F(\omega)$ are shown in Fig. 7, corresponding to the "best" fit models given in Fig. 6 and Table VI. Note that the higher-T_c U_6Fe compound has significantly more weight in the low-frequency end of $F(\omega)$ than the lower-T_c U_6Ni material. It is interesting that experimental data for γ^* and $\Theta\,(T\rightarrow 0)$ roughly correlate and anticorrelate, respectively, with T_c in a number of transition metal materials.[27,30,38,39] Such a trend presumably results from the increased renormalization of long-wavelength acoustic phonons that accompanies an increased electronic density of

TABLE V. Parameters derived from phonon moment analyses of the heat capacities of U_6X compounds. The stated ranges of parameters are representative of the variations incurred when two or three Debye spectra are used, entropy matching at T_c, or proper normalization of the phonon spectrum are enforced or not, etc. These limits should not be considered as true uncertainties in the quoted numbers; rather they provide some estimate of the degree of arbitrariness of the fitting procedure.

Compound	γ^* (mJ/mol K^2)	$\Theta\ (T\rightarrow 0)$ (K)	$\bar{\omega}_{\log}$ (K)	$\langle\omega^{-2}\rangle^{-1/2}$ (K)	$\langle\omega^{-1}\rangle^{-1}$ (K)
U_6Mn	97–104	184–215	92–93	89–90	105
U_6Fe	157	117–118	83	76–78	90–97
U_6Co	133–136	115–124	84–91	78–84	97–119
U_6Ni	92	182–187	99–100	95–97	107–113

TABLE VI. A selection of model parameters derived from phonon moment analyses of the heat capacities of U_6X compounds. Entries are taken from a particular "best" fit of the experimental data. All fits conserve entropy at T_c.

Parameter	U_6Mn	U_6Fe	U_6Co	U_6Ni
γ^*(mJ/mol K^2)	103	157	133	92
Θ_1 (K)	22.2	47.6	22.6	38.3
Θ_2 (K)	68.2	160.5	74.2	132.1
Θ_3 (K)	178.6		250[a]	250[a]
D_1	−0.0040	0.042	0.0026	−0.0060
D_2	0.098	0.958	0.156	0.567
D_3	0.906		0.841	0.439
Θ ($T\to 0$) (K)	215.2	117.4	114.6	181.6
$\langle\omega^{-2}\rangle^{-1/2}$ (K)	89.8	77.5	84.2	97.0
$\langle\omega^{-1}\rangle^{-1}$ (K)	105.3	97.4	~119[b]	113.2
$\exp\langle\ln\omega\rangle$ (K)	117.4	109.4	~147[b]	126.2
$\langle\omega\rangle$ (K)	126.3	116.9	~166[b]	138.3
$\bar{\omega}_2$ (K)	115.3	106.7	~141[b]	125.1
$\bar{\omega}_{\log}$ (K)	92.4	83.3	91.2	100.1
rms deviation	0.99%	0.82%	0.67%	1.5%

[a]Arbitrarily fixed in the fit. The exact value of Θ_3 will not strongly influence the lower-order frequency moments.

[b]Values are not reliable due to a lack of higher-temperature C_P data.

states.[26] Nevertheless, it is still surprising that such an effect could result in the fourfold to fivefold increase in the β coefficient of the T^3 term of the lattice heat capacity noted in comparing the close analogues U_6Mn and U_6Fe, or U_6Ni and U_6Co. This situation suggests that additional terms (e.g., $T^3\ln T$ terms) must be included in

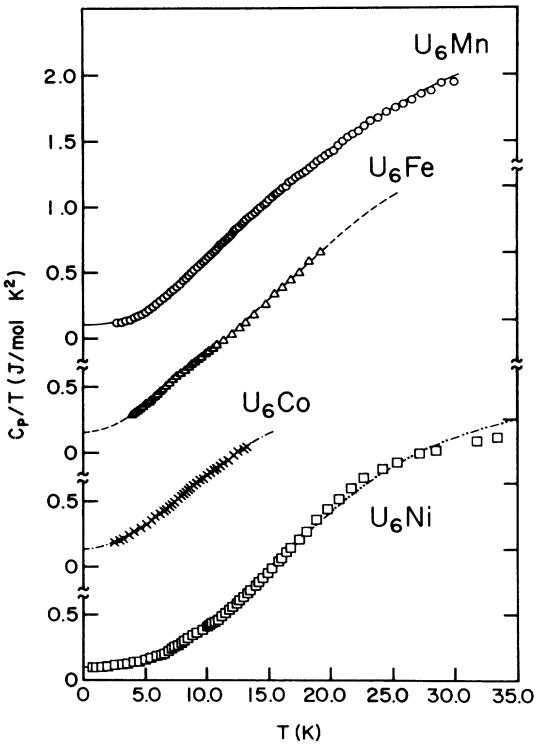

FIG. 6. Heat capacity C_P divided by temperature T vs T for U_6Mn, U_6Fe, U_6Co, and U_6Ni. The symbols represent experimental data at $T > T_c$, and the lines represent a fit of the data using the MOM analysis described in the text. Relevant parameters are collected in Tables V and VI.

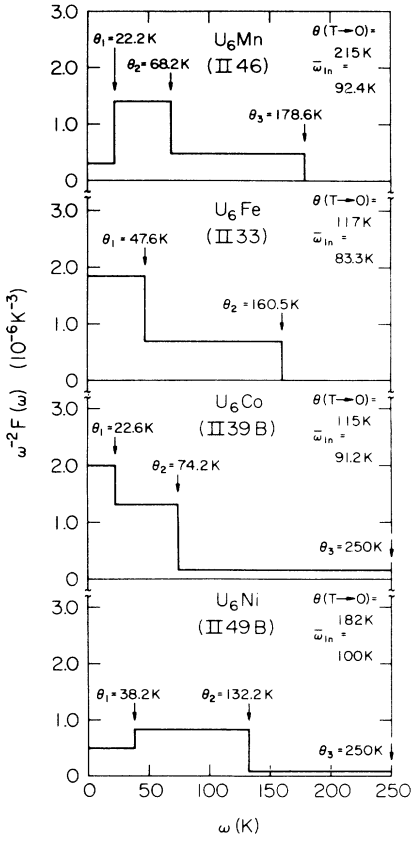

FIG. 7. Approximations to the phonon density of states $F(\omega)$ divided by phonon frequency squared ω^2 vs ω for U_6X ($X \equiv$ Mn, Fe, Co, Ni) compounds. Note that $\omega^{-2}F(\omega)$ is the weighting of the various branches of Debye spectra used in obtaining the MOM fits of $C_P(T)$ detailed in Tables V and VI, and Fig. 6. The Debye cutoffs θ_i for each branch, the relevant values of the effective Debye temperature $\Theta(T\to 0)$, and the approximate Allen-Dynes moment (Ref. 28) $\bar{\omega}_{\log}$ [see Eq. (22)] are shown for each compound.

model fits of the electronic heat capacity. Further experiments, such as inelastic neutron scattering, would be useful to justify such an analysis.

Although the MOM fits to the U_6Mn and U_6Ni data are excellent over a wide range of temperature, there are significant discrepancies between the fits and the data at $T \gtrsim 25$ K. This is particularly noticeable for U_6Ni (see Fig. 6), suggesting that it may be necessary to add Einstein modes to $F(\omega)$ in order to reproduce the extreme negative curvature observed in $C_P T^{-1}$ versus T^2 at higher temperatures. However, the upper cutoffs (θ_3 in Table VI) are not uniquely defined when they are the same order as $\sim 8T_{\max}$, where $T_{\max}$ is the maximum temperature achieved in the measurements. Higher-temperature data, especially for U_6Co and U_6Fe, are required to fully reveal the differences in behavior of the U_6X compounds.

The $C_P T^{-1}$ versus T plots of Fig. 3 emphasize the remarkable differences in low-temperature curvature of C_P between the closely analogous pairs of compounds, U_6Fe and U_6Mn, and U_6Co and U_6Ni. Such differences among analogous compounds have also been observed in Chevrel phases[33,39] Mo_6Se_6 ($T_c = 6.3$ K) and Mo_6S_8 ($T_c = 1.8$ K). Although the magnitude of $C_P(T)$ for the U_6X materials is 1 order of magnitude greater than that of the Chevrel phases, the absolute differences in $C_P T^{-1}$ between higher- and lower-T_c analogues are quite comparable for the two types of materials.

The large γ^* coefficients typically observed in heavy-fermion materials automatically lead to very high entropies at modest temperatures, as demanded by Eq. (1). It is reasonable to associate these large entropies with the presence of "quasilocalized" excitations arising from the hybridization of localized f states with itinerant conduction states.[40,41] It has been pointed out[41] that so far the electronic entropy S_e has only been extracted from calorimetric data for two heavy-fermion compounds (UBe_{13} and U_2Zn_{17}) due to the limited availability of suitable analogue materials that are useful in approximating the lattice contribution C_l. However, it is still very difficult to clearly separate electronic and lattice contributions to the heat capacity, even when suitable analogue compounds (which display a Debye behavior over a significant temperature interval) are available.[42] Recent inelastic neutron scattering measurements[43,44] on UBe_{13} and UPt_3 have provided more direct means for deducing C_l, and surprisingly, these data show no evidence for a "strong coupling" (e.g., phonon softening at low T) between the electron and lattice systems in these two materials.

The four U_6X compounds constitute a unique system of analogues exhibiting reasonably large effective masses and an $\sim 50\%$ variation in γ^*. It is, therefore, of particular interest to compare the variations of the low-temperature S_e of these compounds. A plot of the total entropies $S(T)$ for U_6Mn and U_6Fe are shown in Fig. 8. Note that by $T \approx 15$ K an entropy difference of ~ 2 J/mol K $\sim 0.35R$ ln2 has been established between these compounds. A similar plot, including U_6Mn, U_6Co, and U_6Ni, is shown in Fig. 9. An entropy difference of

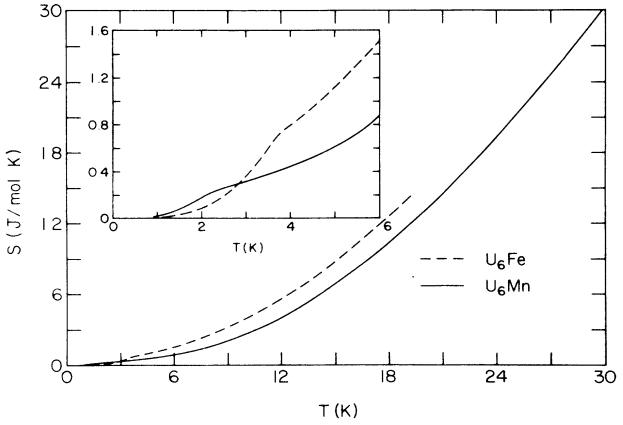

FIG. 8. Total entropy S vs temperature T for U_6Fe and U_6Mn. The inset illustrates the lower-temperature behavior of $S(T)$ below T_c, where $S(T)$ suffers an abrupt change in slope. The curves were calculated using the POLY method, as described in the text.

$\sim 0.45R$ ln2 is established between U_6Co and U_6Ni by $T \approx 13$ K. Note also that these entropy differences appear to saturate with increasing temperature by ~ 15 K, although this conclusion is based on a somewhat limited data set. These entropy differences are remarkable, even if they are normalized to the U concentration. Unfortunately, there is no Th-based, non-5f (and therefore low-γ^*) analogue available for such comparisons. Higher-temperature heat capacity and low-temperature inelastic neutron scattering data would be desirable in order to better quantify these results and confirm the saturation of the entropy differences between various U_6X compounds.

The low-temperature behavior of $C_P(T)$ for the U_6X compounds can be discussed from yet another interesting point of view. DeLong *et al.*[12] reported that the

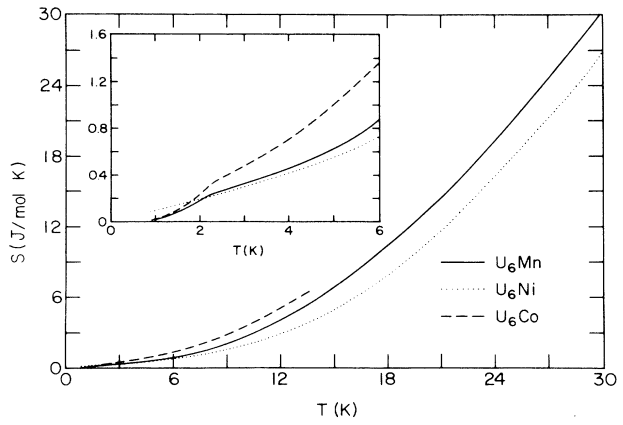

FIG. 9. Total entropy S vs temperature T for U_6Mn, U_6Ni, and U_6Co. The inset illustrates the lower-temperature behavior of $S(T)$, which suffers an abrupt change of slope below T_c in the cases of U_6Mn and U_6Co. The curves were calculated using the POLY method, as described in the text.

normal-state heat capacity of U_6Fe exhibited an unusual T^2 behavior over the temperature range $4 \lesssim T \lesssim 20$ K, as shown in Fig. 10. The solid line in Fig. 10 corresponds to a temperature dependence T^n with $n = 2.06$.

A T^2 dependence of the *lattice* heat capacity C_l has previously been observed in high-T_c $A15$ compounds such as Nb_3Sn and Nb_3Al by Webb *et al.*,[45] and was correlated with a strong T^2 dependence of the electrical resistivity over a similar temperature interval. Webb *et al.* proposed a model phonon density of states $F(\omega)$ that simultaneously reproduced the behavior of both $C_l(T)$ and the T^2 term of the resistivity, suggesting that it arose from electron-phonon scattering in the presence of a high density of low-energy phonon modes. T^2 terms in the low-temperature ($T < 5$ K) resistivities of U_6Fe and U_6Co have been recently observed.[46]

We have intensified our interest in the T^2 behavior of U_6Fe in view of recent observations[47] of a very low-temperature T^2 dependence of $C_P(T)$ for the heavy-fermion material, $CeAl_3$. We anticipated that U_6Co might also display a T^2 character to $C_P(T)$ due to this compound's high γ^* and strong low-frequency weight in $F(\omega)$ (see Fig. 7). Indeed, we have found T^2 behavior, but within two separate temperature intervals, 8 K $\lesssim T \lesssim 13$ K and 2 K $\lesssim T \lesssim 5$ K; We also note that $C_P(T)$ roughly varies as T^n with $n \approx 2.14$ in the interval 5 K $\lesssim T \lesssim 13$ K, demonstrating that the approximate variation of $C_P(T)$ is close to T^2 over the entire normal-state range investigated, 2.3 K $\lesssim T \lesssim 13$ K.

Plots of C_P versus T^2 are given in Fig. 11 for U_6Fe, U_6Co, and U_6Mn. C_P of U_6Mn only roughly follows a T^2 dependence for 10 K $\lesssim T \lesssim 20$ K. If we demand that the total $C_P(T)$ be described by a "simple T^2" law that intersects the origin, we find that U_6Fe obeys such a law at all

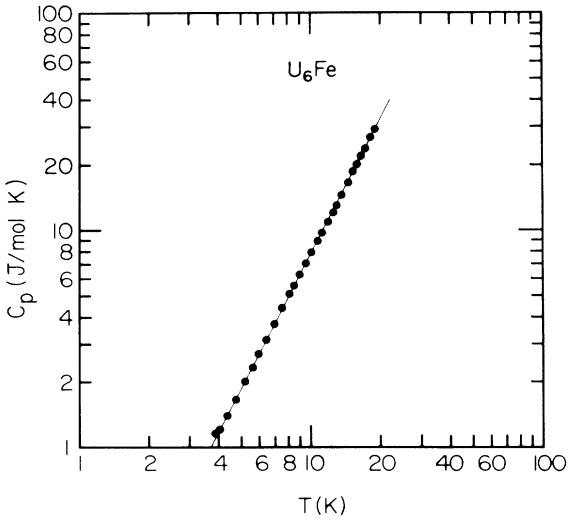

FIG. 10. Logarithm of the normal-state heat capacity C_P vs the logarithm of temperature T for U_6Fe. The straight line is a guide to the eye and represents a T^n dependence of C_P with $n = 2.06$.

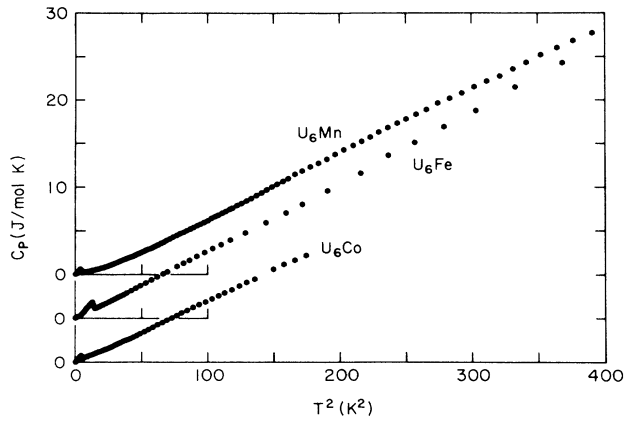

FIG. 11. Heat capacity C_P vs the square of temperature, T^2 for U_6Mn, U_6Fe, and U_6Co.

experimental temperatures $T \geq T_c$, U_6Co satisfies the law less well for $T \geq T_c$, and U_6Mn follows such a dependence only for $T \gtrsim 14$ K. Alternatively, we observe that the region of T^2 behavior may shift to higher temperatures as γ^* decreases. We note that Webb *et al.*[45] observed nonzero intercepts for extrapolations of the T^2 regions of $C_l(T)$ for $A15$ compounds.

We wish to emphasize that the difficulty in separating the lattice and electronic contributions to $C_P(T)$ makes it dangerous to attribute low-energy structure in the experimentally deduced $F(\omega)$ to phonon excitations alone, although this certainly cannot be ruled out. It is possible that a T^2 behavior of $C_P(T)$ may be an artifact of high-γ^* materials for which a clear separation of the lattice contribution is most suspect. For example, we have found that the Mo_6Se_8 and Mo_6S_8 data of Ref. 33 do not exhibit a T^2 phenomenon. This may be associated with the fact that $\gamma^* \lesssim 2.6 \times 10^3$ erg/cm^3 K^2 for these two Chevrel phases,[33,39] 1 order of magnitude smaller than

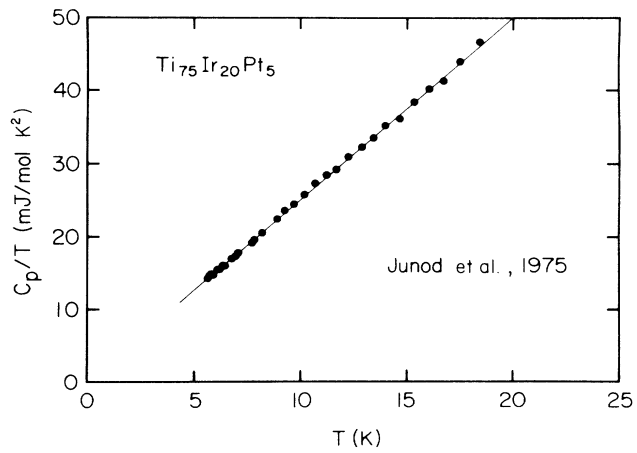

FIG. 12. Normal-state heat capacity C_P divided by temperature T vs T for the pseudobinary $A15$ material $Ti_{0.75}Ir_{0.20}Pt_{0.05}$. The straight line is a guide to the eye. Data were taken from Ref. 48.

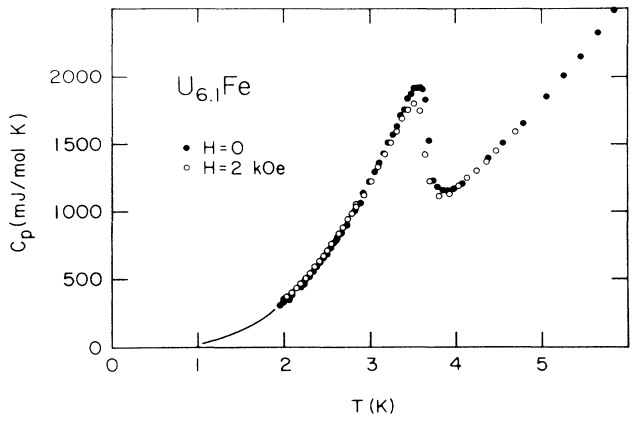

FIG. 13. Heat capacity C_P vs temperature T for U_6Fe in applied magnetic fields $H=0$ and 2 kOe.

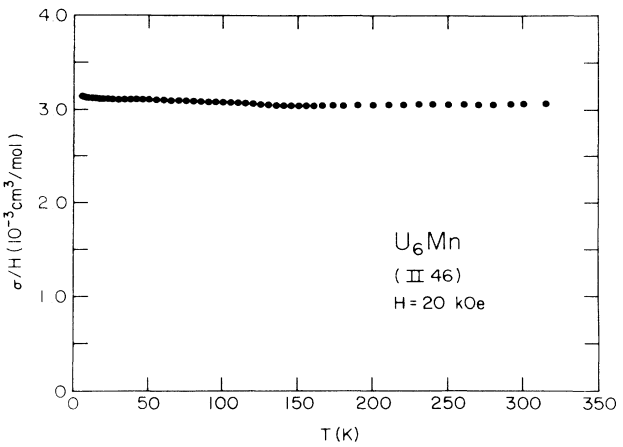

FIG. 15. Magnetization σ divided by applied magnetic field H vs temperature T for U_6Mn. Data were taken in a constant $H=20$ kOe. Traces of ferromagnetism are visible for $T \lesssim 130$ K.

the γ^* of the U_6X compounds. On the other hand, we find that the data of Junod *et al.*[48] for the pseudobinary $A15$ $Ti_{75}Ir_{20}Pt_5$ do follow a T^2 dependence (as shown in Fig. 12); and this material has a $\gamma^* \approx 9\times10^3$ erg/cm^3 K^2, more comparable to the U_6X and high-T_c $A15$ compounds.

Measurements of $C_P(T)$ were also carried out in applied magnetic-field strengths of 2 kOe in the case of U_6Fe and U_6Co, and the results are shown in Figs. 13 and 14. There is no apparent field-induced change in the data, save the small reductions in T_c and ΔC, for a 2 kOe field. Calorimetric determinations of the initial slope of the upper critical field $H'_{c2}(T)$ were made taking care to idealize the transition anomaly in such a manner as to comply with the entropy constraint at T_c. The results are $H'_{c2}(T)=-3.64$ T/K and -3.33 T/K for U_6Fe and U_6Co, respectively. Resistive measurements[12,13] on the same U_6Fe sample II-33 have yielded $H'_{c2}(T_c)=-3.42$ T/K. Menovsky *et al.*[49] have measured the heat capacity of U_6Co in applied fields of 0 to 5 T (in 1 T steps), and found $H'_{c2}(T_c)=-3.7$T/K, $T_c(H=0)=2.3$ K and $\gamma^*(H=0)=126$ mJ/mol K^2, all in very good agreement with our results. DeLong *et al.*[50] have resistively measured two different U_6Co samples and found $H'_{c2}(T_c)=-3.3$ T/K and -3.9 T/K.

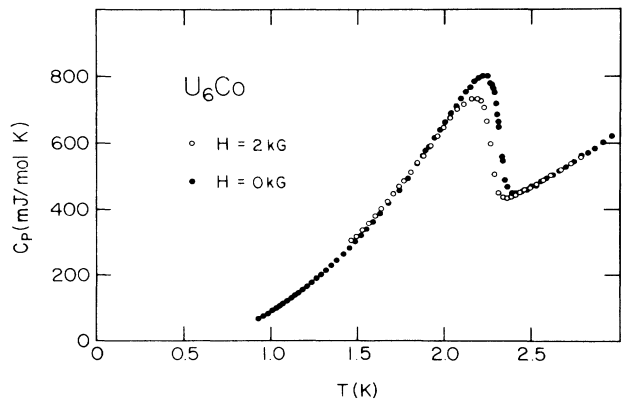

FIG. 14. Heat capacity C_P vs temperature T for U_6Co in applied magnetic fields $H=0$ and 2 kOe.

The relatively large transition width observed for the U_6Mn sample II-46 was attributed to impurities in the U starting materials, and it was therefore useful to measure the magnetic susceptibility of this sample in order to check for temperature-dependent paramagnetism or ferromagnetic impurity phases. Data for the magnetization σ were taken at several temperatures. The susceptibility χ^*, defined by the slope of σ versus H, was found to be temperature independent for 6 K $\leq T \leq 240$ K, but a small remanence developed at $T \lesssim 120$ K. This is confirmed in the plot of σ/H versus T in a fixed field $H=2.0$ T, as shown in Fig. 15. The value of $\sigma/H=3.1\times10^{-3}$ cm^3/mol at $T=6$ K is in excellent agreement with the results of DeLong *et al.*[5] Sample II-46 exhibits about 1 order of magnitude less remanence than their data for U_6Fe sample II-33, suggesting that there were not abnormally large amounts of ferromagnetic phases present in our U_6Mn sample.

V. DISCUSSION OF RESULTS

We now turn to a discussion of possible interpretations of our heat-capacity data. The unusually high values of γ^* and the evidence for a high density of low-energy excitations in the U_6X compounds imply that simple models and traditional interpretations for these data should be regarded with caution. In view of the probable strong $5f$ contributions to the electronic density of states of these materials, several phenomenological models that recently have been applied to heavy-fermion systems are discussed below.

A. Fermi-liquid approach

Several arguments[40,51,52] have been given that imply the superconductivity in heavy-fermion metals should be of an odd-parity type mediated by the exchange of paramagnons. Given that liquid ^{3}He is an exchange-enhanced, triplet-paired superfluid that can also be described as "nearly localized",[53–55] Fermi-liquid theory has frequently been used to compare heavy-fermion superconductors to ^{3}He. Many of these approaches should be carefully distinguished from the microscopic "paramagnon model"[56,57] for exchange-enhanced metals and ^{3}He. Our heat-capacity results have already been used[5] to analyze magnetic susceptibility data for the U_6X compounds in terms of the paramagnon model, and this approach will not be discussed further. We will instead compare our results to recent applications of Landau Fermi-liquid theory to the heavy-fermion problem. The reader is referred to Refs. 41 and 58 for reviews of these techniques.

We are specifically interested in comparing our heat-capacity data with model predictions of the superconducting transition temperature and pairing symmetry. We use the weak-coupling calculation of T_c by Patton and Zaringhalam[59] as outlined by Pethick and Pines.[58] The normal-state properties are described by the symmetric (s) and antisymmetric (a) Landau parameters

$$A_l^{s,a}=\frac{F_l^{s,a}}{1+F_l^{s,a}/(2l+1)} . \tag{27}$$

We assume the forward-scattering sum rule is satisfied in the "*sp* approximation:"[60]

$$\sum_{l=0}^{1}(A_l^s+A_l^a)=0 . \tag{28}$$

The transition temperature is given in terms of a weak-coupling formula for pairing in a state of orbital angular momentum $L=[l(l+1)]^{1/2}\hbar$:

$$^{\mu}T_c=1.13\Theta_c\exp(1/\lambda_{\mu}) , \tag{29}$$

where the pairing interaction strengths in the singlet ($\mu\equiv 0$) and triplet ($\mu\equiv 1$) channels are given by

$$\lambda_0=\sum_l\frac{(-1)^l}{4}(A_l^s-3A_l^a) ,$$
$$\lambda_1=\sum_l\frac{(-1)^l}{12}(A_l^s+A_l^a) . \tag{30}$$

Θ_c is a cutoff that must satisfy $^{\mu}T_c\ll\Theta_c\ll T_F^*$ in the weak-coupling limit.[41] Note that in the *sp* approximation the sums in Eq. (30) are taken only over $l=0,1$, and λ_{μ} must be less than zero for an attractive interaction and nonzero T_c to occur.

We will discuss our attempts to apply Eqs. (27)–(30) to our data using four different types of approximations. The first method was used by Valls and Tesanovic[61] in a direct application of the "almost localized" model of ^{3}He to heavy-fermion superconductors. The assumption of a large m^*/m_e and incipient localization imply $A_1^s\sim 3$, $A_0^s\sim 1$, and $A_0^a\sim -3$, and the sum rule [Eq. (30)] is used to obtain $A_1^a=-1$. Equations (30) then yield $\lambda_0=1$ and $\lambda_1=-\frac{1}{3}$, and thereby predict triplet superconductivity. It is customary[58] to reexpress Θ_c in terms of either the Fermi or spin-fluctuation temperatures:

$$1.13\Theta_c=\delta T_F^*=\beta T_{\rm sf} . \tag{31}$$

δ and β are unknown scaling factors, and it is assumed that $T_{\rm sf}=(1+F_0^a)T_F^*$.[58] A summary of experimental parameters for the four U_6X compounds is given in Table VII, and a list of parameters derived from the "almost localized" model is given in Table VIII.

The method used by Valls and Tesanovic suffers from several serious defects. It assumes Galilean invariance within the Fermi liquid and sets $m^*/m_e=1+F_1^s/3$, implying $A_1^s\sim 3$ for heavy fermions. However, the Bloch symmetry of crystals invalidates the relation between m^*/m_e and F_1^s.[41,58] Further, the m^* values of the U_6X compounds are roughly 1 order of magnitude less than those of UPt_3 and UBe_{13}, and the assumption of $A_1^s\sim 3$ is probably not justified in our case.

A second method, which we label the "induced interaction" approach,[58,62,63] relies on a general treatment of the Landau interaction function in the case of a short-range potential between quasiparticles.[64,65] We assume $A_0^s\sim 1$ for a charged Fermi liquid,[58] and the effective mass is given by

$$m^*/m_b=1+F_1^s/3 , \tag{32}$$

where m_b is the quasiparticle mass in the absence of "backflow,"[62,63] and contains renormalizations due to band structure and the electron-phonon interaction. The quasiparticle mass m_b can be measured in the superconducting state via observation of the London penetration depth.[63] The essential point is that this approach does not rely on Galilean invariance of the Fermi liquid. Unfortunately, the practical application of the model is best achieved by fixing F_0^a and A_0^a with the $T^3\ln T$ contribution to C_P, such as is possible in the case of ^{3}He, UPt_3, and UAl_2.[58] Since very few materials unambiguously exhibit the $T^3\ln T$ term (the U_6X compounds evidently do not), one must adopt another means of fixing F_0^a.

We have chosen to relate F_0^a to the "R ratio" for a spin-$\frac{1}{2}$ Fermi liquid:

$$R=\frac{1}{3}\left[\frac{\pi k_B}{\mu_B}\right]^2\frac{\chi^*(T\to 0)}{\gamma^*}\sim(1+F_0^a)^{-1} . \tag{33}$$

The validity of this relation has been discussed[5] in ap-

TABLE VII. Experimental parameters for Fermi-liquid models of the U_6X compounds.

Compound	T_c (K)	R	k_F[a] (10^8 cm^{-1})	m^*/m_e[a]	T_F^*[a] (K)
U_6Mn	2.21	2.2	1.56	15	7200
U_6Fe	3.70	1.4	1.57	23	4690
U_6Co	2.29	1.5	1.57	20	5540
U_6Ni	0.35	2.4	1.565	13.5	8020

[a]Based on an estimate of $Z=3$ fermions per U atom.

TABLE VIII. Parameters derived from an "almost localized" Fermi-liquid model.

Compound	Θ_c (K)	δ	λ_0	λ_1
U_6Mn	39	6.2×10^{-3}	1	$-\frac{1}{3}$
U_6Fe	66	1.6×10^{-2}	1	$-\frac{1}{3}$
U_6Co	41	8.3×10^{-3}	1	$-\frac{1}{3}$
U_6Ni	6.2	8.8×10^{-4}	1	$-\frac{1}{3}$

plication to heavy-fermion systems. The major risks in using Eq. (33) stem from its omission of band-structure and spin-orbit effects on the magnetic susceptibility χ^*. However, these approximations are certainly consistent with those used in the majority of Fermi-liquid models.[41]

The "induced interaction" approach yields, in the case of U_6Fe, $\lambda_1=0.1$, thereby precluding a triplet pairing state, and $\lambda_0=0.1-A_1^s$. A_1^s cannot be determined from Eq. (32) without knowledge of m_b. Assuming $1\lesssim m_b/m_e\lesssim 14$, we deduce $1.2\lesssim A_1^s\lesssim 2.9$ and $-2.8\lesssim\lambda_0\lesssim -1.1$. However, these parameters imply $4.7\ \text{K}\lesssim\Theta_c\lesssim 8.1$ K, indicating a breakdown of the weak-coupling assumption due to the proximity of Θ_c to T_c. On the other hand, $A_1^s>0.1$ is required for a finite T_c. We can only conclude that $1<m_b/m_e\lesssim 22$ with $10^{-3}<\delta$, and that $1\lesssim m^*/m_b<2$ in order for the weak-coupling approximation to be valid.

A third approach was recently suggested by Varma,[40] and postulates that the momentum dependence of the quasiparticle self-energy is negligible compared to its energy dependence. m^* is then dominated by a strong wave-function renormalization (SWR) that yields no effect on a number of transport properties, similar to the electron-phonon interaction in metals.[66] The SWR approach results in an explicit relationship between m^* and F_0^s:

$$\frac{m^*}{m_e}=1+F_0^s\ . \tag{34}$$

We have applied the SWR method to our U_6Fe data and deduced $A_0^a=-0.40$, $A_0^s=0.96$, $\lambda_1=0.09$, and $\lambda_0=0.12-A_1^s$, in good agreement with the induced-interaction approach parameters calculated above. Therefore, depending on the proper value of A_1^s, the weak-coupling approximation may again be violated within this method. It is noteworthy that recent experiments[46] on the upper critical field and magnetoresistance of UPt_3, U_6Fe, and U_6Co have provided independent evidence for anomalously low values of a cutoff energy comparable to T_c, and a failure of the weak-coupling approximation for heavy-fermion superconductors.

Finally, we have elaborated on a conjecture of Pethick and Pines[58] that a "law of corresponding states" (LCS) may apply to the Fermi-liquid properties of ^{3}He, UPt_3, and other heavy-fermion materials. We assume $A_0^s\sim 1$ and that the scaling parameter β of Eq. (31) is 0.05 for all Fermi liquids of interest. Again using Eq. (33), we deduce the parameters summarized in Table IX. Note that singlet pairing is predicted for all four U_6X com-

TABLE IX. Comparison of Fermi-liquid parameters for U_6X, ^{3}He, and UPt_3. Parameters for ^{3}He and UPt_3 are taken from Refs. 53 and 58. The parameters for the U_6X materials are derived using the "LCS" method described in the text.

Material	k_F (Å^{-1})	T_F^* (K)	m^*/m_e	A_0^s	A_0^a	A_1^s	T_{sf} (K)	δ	β	Θ_c (K)	λ_0	λ_1
^{3}He	0.8	1.7	2.7	0.9	−2.3	1.9	0.51	0.015	0.05	0.022	1.1	−0.23
^{3}He (30 kbar)		1.1	~5	0.98	−3.2	~2.4	0.26	0.012	0.05	0.012	1.9	−0.37
UPt_3	1.08	287	180	≡1.0	−4.3	~2.6	55	0.01	0.05	2.4	3.4	−0.55
UPt_3 (8.9 kbar)	1.08	370	161	≡1.0	−3.4		85	0.011	0.05	3.8		−0.40
U_6Mn	1.56	7200	15	≡1.0	−1.2	1.5	3240	0.023	≡0.05	143	−0.23	−0.03
U_5Fe	1.57	4690	23	≡1.0	−0.40	0.36	3330	0.035	≡0.05	148	−0.26	0.10
U_6Co	1.57	5540	20	≡1.0	−0.43	0.37	3880	0.030	≡0.05	172	−0.23	0.095
U_6Ni	1.565	8020	13.5	≡1.0	−1.4	1.8	3340	0.021	≡0.05	148	−0.16	−0.07

pounds (triplet T_c's are extremely low, whenever $\lambda_1 < 0$), although these materials appear to be near a crossover to the triplet state. Note also that the values of Θ_c for the U_6X compounds justify the weak-coupling formula, and that $\Theta_c \ll T_{sf}$, suggesting that paramagnon pairing is "cut off"[51] by a lower-energy excitation such as phonons.

Several caveats to the above Fermi-liquid analyses should be mentioned. Band-structure effects arising from a breakdown of Galilean invariance lead to a "bare band mass" and orbital contributions to χ^* that either have been neglected or only roughly approximated in our analyses. Spin-orbit and anisotropy effects are also omitted, and the weak coupling Eq. (29) should not be trusted for calculation of accurate values of relevant parameters.[41] The parameters k_F, m^*, and T_F^* are also uncertain since they depend upon a proper choice of the fermion density n, which is not easily determined from independent measurements. Pethick and Pines[57] and DeLong[67] have given phenomenological arguments for assuming that each U atom contributes three "heavy fermions" (other contributions to n are neglected). We have adopted this assumption given the lack of direct experimental measurements of n and our desire to express our results within a common convention used by other authors.

In spite of the many approximations that one is forced to make in the application of Fermi-liquid theory, the various models discussed above generally yield quite reasonable values for the Landau parameters and associated quantities. At present there is no accepted microscopic model for heavy-fermion metals, and it is therefore useful to compare the Fermi-liquid properties of the U_6X compounds to those of related materials. We believe that the relative trends and semiquantitative results given in Table IX have physical significance.

B. Strong-coupling analysis

The results of the Fermi-liquid analyses suggest that even-parity superconductivity due to the usual electron-phonon interaction is probably appropriate to the U_6X compounds. The large size of the specific-heat jump at T_c and the zero-temperature thermodynamic critical field for U_6Co and U_6Fe (see Tables III and IV) imply that our results should be analyzed with a theoretical model that takes into account strong-coupling effects. We have accordingly compared our data to the Allen-Dynes model[28] in order to extract values of the electron-phonon coupling λ [see Eq. (19)] and the band-structure density of states $N_b(E_F)$ given by

$$N_b(E_F)=\frac{N^*(E_F)}{1+\lambda}=\frac{3\gamma^*}{2\pi^2 k_B^2(1+\lambda)} . \tag{35}$$

λ must be deduced from the T_c formula [Eq. (17)] using the approximation $\omega_{\log}\approx\bar{\omega}_{\log}$ [see Eqs. (18) and (20)] and the functions f_1 and f_2 defined by

$$f_1=[1+(\lambda/\Lambda_1)^{3/2}]^{1/3} \tag{36}$$

and

$$f_2=1+\frac{\lambda^2(\bar{\omega}_2/\omega_{\log}-1)}{\lambda^2+\Lambda_2^2} , \tag{37}$$

TABLE X. Parameters for the strong-coupling analysis of the U_6X compounds. All parameters calculated assuming $\mu^*=0.13$.

Compound	f_1	f_2	λ	$N_b(E_F)$ (eV-atom-spin)$^{-1}$
U_6Mn	1.03	1.01	0.668	1.85
U_6Fe	1.04	1.01	0.841	2.58
U_6Co	1.03	1.01	0.678	2.40
U_6Ni	1.01	1.00	0.437	1.94

where

$$\Lambda_1=2.46(1+3.8\mu^*) \tag{38}$$

and

$$\Lambda_2=1.82(1+6.3\mu^*)\bar{\omega}_2/\omega_{\log} . \tag{39}$$

We assume a typical value $\mu^*=0.13$ and initially set $f_1\approx f_2\approx 1$ in order to arrive at an initial estimate or λ using the phonon moment values in Table VI and T_c's from Table III. The estimate of λ is then used to recalculate f_1, f_2, and λ in an iterative procedure until they converge to self-consistent values. The results of the iteration are given in Table X.

Values of λ for the U_6X compounds are large but reasonable. On the other hand, the values of $N_b(E_F)$ for the U_6X compounds are approximately 1 order of magnitude larger than those of typical transition metal compounds, and are several times larger than for high-T_c $A15$ materials.[68] If we use the relation

$$m^*=(1+\lambda)m_b , \tag{40}$$

where m_b is the average "bare band-structure" mass, we conclude that $m_b \gtrsim 10m_e$ for the U_6X compounds. These are remarkably large masses considering that they are obtained in the approximation of a spherically averaged $N^*(E_F)$. However, Leggett,[69] has pointed out that Eq. (40) may not be valid for heavy-fermion materials. Moreover, the large $N^*(E_F)$ found in the U_6X materials would normally imply a very high T_c, indeed. It is therefore reasonable to postulate that some "repulsive" mechanism prevents T_c from exceeding ~ 4 K in U_6Fe.

VI. CONCLUDING REMARKS

We have already mentioned several similarities between the high-T_c Chevrel, $A15$, and U_6X compounds. However, the behavior of narrow-d-band materials is far from understood,[70,71] and a strict analogy between $A15$ and $5f$-band or heavy-fermion compounds cannot presently be constructed. It is nevertheless important to point out some of the paradoxes or difficulties that remain in attaining a unified picture of materials whose bandwidth is intermediate between that of UBe_{13} and conventional BCS superconductors such as Al or Sn.

Here, it is instructive to compare U_6Fe with the $A15$ compound V_3Ga, which has a $T_c=15$ K, a value that is comparable to, or less than, that of the highest-T_c materials of this class. However, the γ^* value of V_3Ga is ap-

proximately double that of the higher-T_c $A15$'s (Refs. 30 and 68) and is comparable to that of U_6Fe.[12] The evidence for a strong Pauli limiting of H_{c2} for V_3Ga (Ref. 68) suggests that paramagnons may be the appropriate mechanism responsible for the suppression of the superconducting properties of this compound. Indeed, phenomenological arguments[67,71] imply that magnetic interactions strongly suppress superconductivity for $N^*(E_F)$ values slightly larger than those observed for the U_6X and V_3Ga compounds.

However, applying the same line of reasoning to the U_6X materials does not yield a straightforward explanation of their anomalous properties. In particular, no clear evidence has yet been found that the H_{c2} of U_6Fe is at all Pauli limited; indeed, the temperature dependences of H_{c2} for U_6Fe and U_6Co exhibit unusual positive curvature and low-temperature values that are significantly *greater* than expected.[46,50] Further, one must also simultaneously explain why lower T_c's and *larger* values of the susceptibility enhancement ratio R are correlated with *smaller* $N^*(E_F)$ in these materials[71] (see Tables VII and X). Note that considerable difficulties have been encountered in explaining similar effects in $A15$ materials.[68]

We have neglected exotic or complex contributions to the heat capacity in our analyses. It is possible that anharmonic corrections (e.g., "phonon softening") can account for the unusual behavior of the U_6X materials, as has been suggested for $A15$ materials.[26,72] Subtle low-temperature phase transitions[6,73,74] and polaronic[75–78] effects are also possible mechanisms for anomalous behavior in these materials.

A complete analysis of the heat capacity of the U_6X compounds, including a well-defined separation of the electronic and lattice contributions, may prove particularly difficult in view of the breakdown of adiabaticity inferred from the heat-capacity behavior of a number of narrow-band materials.[5,67,70,71,79] The properties of the U_6X compounds and their incomplete parallels with $A15$ and Chevrel compounds remain enigmatic and deserve further study.

ACKNOWLEDGMENTS

The research at University of California at San Diego was supported by the U.S. Department of Energy under Grant No. DE-FG03-86ER45230. Research at the University of Kentucky was supported by a grant from Research Corporation (New York, NY).

*Present address: Department of Physics, Virginia Commonwealth University, Richmond, VA 23284-0001.

[1]B. S. Chandrasekhar and J. K. Hulm, J. Phys. Chem. Solids **7**, 259 (1958).
[2]L. F. Bates and J. R. Mallard, Proc. R. Soc. London **63B**, 520 (1950).
[3]P. Gordon, D.Sc. thesis, Massachussetts Institute of Technology, 1952. (Also available at United States Atomic Energy Commission, Report No. AECU-1833, 1982 and Technical Information Service, Oak Ridge, TN, 1982.)
[4]V. V. Gann, A. I. Skvortsov, and A. van den Bosch, Phys. Status Solidi A **41**, 225 (1977).
[5]L. E. DeLong, R. P. Guertin, S. Hasanain, and T. Fariss, Phys. Rev. B **31**, 7059 (1985).
[6]L. E. DeLong, G. W. Crabtree, L. N. Hall, H. Kierstead, H. Aoki, S. K. Dhar, K. A. Gschneidner, Jr., and A. Junod, Physica **135B**, 81 (1985).
[7]B. T. Matthias, J. Appl. Phys. **31**, Suppl., 23S (1960).
[8]H. H. Hill and B. T. Matthias, Phys. Rev. **168**, 464 (1968).
[9]B. T. Matthias, C. W. Chu, E. Corenzwit, and D. Wohlleben, Proc. Nat. Acad. Sci. U.S.A. **64**, 459 (1969).
[10]B. T. Matthias, J. Phys. (Paris) Colloq. **32**, C1-607 (1971).
[11]L. E. DeLong, J. G. Huber, K. N. Yang, and M. B. Maple, Bull. Am. Phys. Soc. **27**, 157 (1982).
[12]L. E. DeLong, J. G. Huber, K. N. Yang, and M. B. Maple, in *Superconductivity in d- and f-Band Metals 1982*, edited by W. Buckel and W. Weber (Kernforschungszentrum Karlsruhe GmbH, Karlsruhe, 1982), pp. 467–471.
[13]L. E. DeLong, J. G. Huber, K. N. Yang, and M. B. Maple, Phys. Rev. Lett. **51**, 312 (1983).
[14]U. Rauchschwalbe, W. Lieke, C. D. Bredl, F. Steglich, J. Aarts, K. M. Martini, and A. C. Mota, Phys. Rev. Lett. **49**, 1448 (1982).
[15]D. D. Koelling, B. D. Dunlap, and G. W. Crabtree, Phys. Rev. B **31**, 4966 (1985).
[16]G. R. Stewart, Rev. Mod. Phys. **56**, 755 (1984).
[17]H. R. Ott, H. Rudigier, Z. Fisk, and J. L. Smith, Phys. Rev. Lett. **50**, 1595 (1983).
[18]G. R. Stewart, Z. Fisk, J. O. Willis, and J. L. Smith, Phys. Rev. Lett. **52**, 679 (1984).
[19]N. C. Baenziger, R. E. Rundle, A. I. Snow, and A. S. Wilson, Acta Crystallogr. **3**, 34 (1950).
[20]J. J. Engelhardt, J. Phys. Chem. Solids **36**, 123 (1975).
[21]R. W. White, J. D. G. Lindsay, and R. D. Fowler, Solid State Commun. **13**, 531 (1973).
[22]See N. Ashcroft and D. Mermin, *Solid State Physics* (Saunders College, Philadelphia, 1976), Chaps. 22 and 25.
[23]E. R. Gopal, *Specific Heats At Low Temperature* (Plenum, New York, 1965), Chap. 2.
[24]H. R. Ott, H. Rudigier, Z. Fisk, and J. L. Smith, Phys. Rev. B **31**, 1651 (1985).
[25]E. A. Lynton, *Superconductivity* (Methuen, London, 1969).
[26]G. S. Knapp, J. Less-Common Met. **62**, 127 (1978), and references therein.
[27]A. Junod, D. Bichsel, and J. Muller, Helv. Phys. Acta **52**, 580 (1979).
[28]P. B. Allen and R. C. Dynes, Phys. Rev. B **12**, 905 (1975).
[29]A. Junod, Solid State Commun. **33**, 55 (1980).
[30]A. Junod, T. Jarlborg, and J. Muller, Phys. Rev. B **27**, 1568 (1983).
[31]A. Junod, J. L. Jorda, M. Pelizzone, and J. Muller, Phys. Rev. B **29**, 1189 (1984).
[32]G. S. Knapp, S. D. Bader, and Z. Fisk, Phys. Rev. B **13**, 3783 (1976).
[33]N. E. Alekseevskii, N. M. Dobrovolskii, G. Wolf, C. Hohlfeld, and K. Bohmhammel, J. Less-Common Met. **62**, 329 (1978).
[34]M. A. Biondi, A. T. Forrester, M. P. Garfunkel, and C. B. Satterthwaite, Rev. Mod. Phys. **30**, 1109 (1958).

[35]A. W. Overhauser and J. Appel, Phys. Rev. B **31**, 193 (1985).
[36]H. R. Ott, H. Rudigier, T. M. Rice, K. Ueda, Z. Fisk, and J. L. Smith, Phys. Rev. Lett. **52**, 1915 (1984).
[37]T. M. Rice, K. Ueda, H. R. Ott, and H. Rudigier, Phys. Rev. B **31**, 594 (1985).
[38]G. F. Syrykh, M. G. Zemlyanov, N. A. Chernoplekov, and B. I. Savel'ev, Zh. Eksp. Teor. Fiz. **81**, 308 (1981) [Sov. Phys.–JETP **54**, 165 (1981)].
[39]B. Lachal, A. Junod, and J. Muller, J. Low Temp. Phys. **55**, 195 (1984).
[40]C. M. Varma, Phys. Rev. Lett. **55**, 2723 (1985).
[41]P. A. Lee, T. M. Rice, J. W. Serene, L. J. Sham, and J. W. Wilkins, Comments Cond. Mater. Phys. **12**, 99 (1986).
[42]L. E. DeLong, J. Less-Common Met. **127**, 285 (1987).
[43]R. A. Robinson, J. D. Axe, A. I. Goldman, Z. Fisk, J. L. Smith, and H. R. Ott, Phys. Rev. B **33**, 6488 (1986).
[44]B. Renker, F. Gompf, J. B. Suck, H. Rietschel, and P. Frings, Physica **136B**, 376 (1986).
[45]G. W. Webb, Z. Fisk, J. J. Engelhardt, and S. D. Bader, Phys. Rev. B **15**, 2624 (1977).
[46]L. E. DeLong, G. W. Crabtree, L. N. Hall, D. G. Hinks, W. K. Kwok, and S. K. Malik, Phys. Rev. B **36**, 7155 (1987).
[47]G. E. Brodale, R. A. Fisher, N. E. Phillips, and J. Flouquet, Phys. Rev. Lett. **56**, 390 (1986).
[48]A. Junod, R. Flukiger, and J. Muller, J. Phys. Chem. Solids **37**, 27 (1976).
[49]A. Menovsky, J. C. P. Klaasse, R. Verhoef, and J. J. M. Franse, in Proceedings of the 14th Conference on Actinides, Davos, 1984, edited by J. Schoenes (unpublished), p. 131.
[50]L. E. DeLong, L. N. Hall, S. K. Malik, G. W. Crabtree, W. Kwok, and K. A. Gschneider, Jr., J. Magn. Magn. Mater. **63&64**, 478 (1987).
[51]P. W. Anderson, Phys. Rev. B **30**, 1549 (1984).
[52]M. T. Béal-Monod, Phys. Rev. B **31**, 1647 (1985).
[53]K. Levin and O. T. Valls, Phys. Rep. **98**, 1 (1983).
[54]D. Vollhardt, Rev. Mod. Phys. **56**, 99 (1984).
[55]P. C. E. Stamp, J. Phys. F **15**, 1829 (1985).
[56]S. Doniach and S. Engelsberg, Phys. Rev. Lett. **47**, 750 (1966).
[57]W. F. Brinkman and S. Engelsberg, Phys. Rev. **169**, 417 (1968).
[58]C. J. Pethick and D. Pines, in *Novel Superconductivity,* edited by S. A. Wolf and V. Z. Kresin (Plenum, New York, 1987).
[59]B. R. Patton and A. Zaringhalam, Phys. Lett. **55A**, 95 (1975).
[60]K. S. Dy and C. J. Pethick, Phys. Rev. **185**, 373 (1969).
[61]O. T. Valls and Z. Tesanovic, Phys. Rev. Lett. **53**, 1497 (1984).
[62]K. S. Bedell and K. F. Quader, Phys. Rev. B **32**, 3296 (1985).
[63]K. S. Bedell, J. Less-Common Met. **127**, 299 (1987).
[64]S. Babu and G. E. Brown, Ann. Phys. (N.Y.) **78**, 1 (1973).
[65]T. L. Ainsworth, K. S. Bedell, G. E. Brown, and K. F. Quader, J. Low Temp. Phys. **50**, 319 (1983).
[66]R. E. Prange and L. P. Kadanoff, Phys. Rev. **134**, A566 (1964).
[67]L. E. DeLong, J. Magn. Magn. Mater. **62**, 1 (1986).
[68]T. P. Orlando and M. R. Beasley, Phys. Rev. Lett. **46**, 1598 (1981).
[69]A. J. Leggett, J. Magn. Magn. Mater. **63&64**, 406 (1987).
[70]P. W. Anderson and C. C. Yu, in *Highlights in Condensed Matter Theory,* Proceedings of the International School of Physics "Enrico Fermi," Course LXXXIX, Varena, 1985, edited by F. Bassani, F. Fumi, and M. P. Tosi (North-Holland, Amsterdam, 1985), pp. 767–797.
[71]L. E. DeLong, in *Theoretical and Experimental Aspects of Valence Flucutations and Heavy Fermions,* edited by L. C. Gupta and S. K. Malik (Plenum, New York, 1987), pp. 65–76; in *Novel Superconductivity,* edited by S. A. Wolf and V. Z. Kresin (Plenum, New York, 1987), pp. 253–264.
[72]G. S. Knapp, S. D. Bader, and Z. Fisk, Phys. Rev. B **13**, 3783 (1976).
[73]C. W. Kimball, P. P. Vaishnava, A. E. Dwight, J. D. Jorgensen, and F. Y. Fradin, Phys. Rev. B **32**, 4419 (1985).
[74]G. Lemon, P. Boolchand, M. Stevens, M. Marcuso, L. E. DeLong, and J. G. Huber, J. Less-Common Met. **127**, 329 (1987).
[75]A. S. Alexandrov, J. Ranninger, and S. Robaszkiewicz, Phys. Rev. B **33**, 4526 (1986).
[76]S. H. Liu, Phys. Rev. Lett. **58**, 2706 (1987).
[77]K. A. Kikoin and D. I. Khomskii, Pis'ma Zh. Eksp. Teor. Fiz. **45**, 396 (1987) [JETP Lett. **45**, 505 (1987)].
[78]A. S. Aleksandrov, V. N. Grebenev, and E. A. Mazur, Pis'ma Zh. Eksp. Teor. Fiz. **45**, 357 (1987) [JETP Lett. **45**, 455 (1987)].
[79]L. E. DeLong, Phys. Rev. B **33**, 3556 (1986).